Strain determination in ultrathin bcc Fe layers on Si(001) by x-ray diffraction

P. Bertoncini, P. Wetzel,* D. Berling, A. Mehdaoui, B. Loegel, J. C. Peruchetti, and G. Gewinner
Laboratoire de Physique et de Spectroscopie Electronique, UPRES, A 7014 CNRS,
4 rue des Frères Lumiére, 68 093 Mulhouse cedex, France

V. Pierron-Bohnes
Institut de Physique et de Chimie des Matériaux de Strasbourg, Groupe d'Etudes des Matériaux Métalliques,
23, rue du Loess, 67037 Strasbourg cedex, France

J. F. Bérar and H. Renevier
Laboratoire de Cristallographie, CNRS-Université Joseph Fourier, Grenoble, France
and ESRF, Grenoble, France
(Received 25 June 2001; revised manuscript received 17 October 2001; published 5 April 2002)

Good quality body-centered cubic iron layers can be grown on Si(001) at room temperature using thin $FeSi_2$ or $CoSi_2$ silicide buffer layers. The in-plane and out-of-plane strains are measured by x-ray diffraction (XRD). Due to the difference in Fe and Si parameters of $+5.6\%$, the thin Fe layers undergo a strong tetragonal distortion. For the samples deposited on $FeSi_2$, the measured biaxial in-plane compressive strain ranges from values as large as -3.8% in the thinnest films (<25 ML) to -1% in the thicker layers (>40 ML). In the samples deposited on $CoSi_2$, a part of the iron layer clearly observable up to 40 ML, apparently grows in pseudomorphy with the silicon, whereas another dominant part above 15 ML partly relaxes and behaves as on $FeSi_2$ templates but with systematically larger strains. The evolution of the in-plane cubic effective magnetic anisotropy constant versus Fe film thickness observed in previous work, can be explained by means of fourth-order (in spin) magnetoelastic coupling in the iron lattice with the strain components determined by XRD. Finally, the observed ratio between the perpendicular and in-plane strain components differs substantially from linear elasticity theory predictions and indicates the importance of anharmonic effects and/or defects in the description of the elastic properties of such films.

DOI: 10.1103/PhysRevB.65.155425 PACS number(s): 68.55.−a, 61.10.−i, 75.70.−i

INTRODUCTION

The growth of ferromagnetic thin layers on semiconductor surfaces has recently received increased attention due to the potential application of magnetoelectronic devices in the silicon technology and for the study of fundamental magnetic properties.[1–6] Actually, interest in epitaxial growth of ultrathin $3d$ transition metal films on semiconductor single-crystal substrates arises from the opportunity to stabilize specific crystalline structure caused by misfit strain. These layers may exhibit unusual electronic and magnetic properties (magnetic moment, Curie temperature, magnetic anisotropy, etc.) significantly modified compared to those in bulk materials. The tailoring of such magnetic layers requires a detailed knowledge of the correlation among magnetic, structural, and morphological properties. To understand the magnetic anisotropy behavior, one of the most important structural parameters to be investigated is the lattice strain produced in the films by the coherency stress imposed by the Si substrate in the plane of the interface.

Previous studies of the growth of Fe on Si(001) have shown that epitaxial overlayers do not form at room temperature (RT).[7–10] A spontaneous and significant chemical intermixing occurs between the Fe overlayer and the Si substrate. For subsequent Fe deposits, the Si dissolution in the overlayer decreases and a metallic polycrystalline Fe layer develops. However, such films exhibit a decreasing magnetization when decreasing the film thickness.[11] Ferromagnetism disappears for a Si concentration close to FeSi.[12]

Despite the fairly large misfit $(+5.6\%)$ between Fe and Si lattices, successful epitaxial growth of high-quality Fe films was recently achieved at room temperature by use of a thin epitaxial Co or Fe disilicide template layer.[13] This template grown on the (001) silicon surface prior to the Fe deposition, strongly reduces the Fe/Si intermixing and permits the epitaxial growth of Fe at RT.

Structural characterization of these Fe films was performed by low-energy electron diffraction, inelastic medium-energy electron diffraction, x-ray photoelectron diffraction (XPD) and *ex situ* high-resolution transmission electron microscopy (HRTEM), while the magnetic properties were studied at RT by magneto-optical Kerr effect (MOKE).[13–15] In particular, it was established that iron grows in the body-centered cubic (bcc) structure with the epitaxy relations Fe(001)[100]/Si(001)[100] and with a marked tetragonal distortion in the thinnest films. Epitaxial iron on Si(001) is under a biaxial compressive stress due to the lattice mismatch in their RT bulk forms: $u_0=(2a_0^{\mathrm{Fe}}-a_0^{\mathrm{Si}})/a_0^{\mathrm{Si}}=5.6\%$. The lattice mismatch gives rise to isotropic strain in the (001) plane $(e_{xx}=e_{yy}=e_{\|})$, and to an out-of-plane tensile strain often assumed to follow the linear continuum elasticity Poisson law: $e_{\perp}=-2(C_{12}/C_{11})e_{\|}$ where C_{IJ} are the usual elastic constants.

In these previous studies the in-plane strain of Fe layers was qualitatively investigated using HRTEM.[14] MOKE measurements at RT have shown the appearance of RT magneti-

 ©2002 The American Physical Society

zation for the deposition of about four Fe monolayers (ML). In addition, Fe films evaporated at normal incidence show a ferromagnetic order with in-plane magnetization and fourfold symmetry anisotropy.[14,15] The relevant effective anisotropy constant was measured as a function of the Fe thickness and found to change its sign near 20 ML. The origin of this behavior was investigated by means of a Néel-type pair interaction model and was mainly traced back to higher-order magnetoelastic effects related to the biaxial in-plane compressive strain in the whole film induced by the Fe and Si lattice misfit.[15]

In this paper, we describe the measurement of the lattice strain versus film thickness in epitaxial Fe films grown at normal incidence at RT on both $FeSi_2/Si(001)$ and $CoSi_2/Si(001)$ substrates. Both in-plane and out-of-plane elastic strains were measured using synchrotron x-ray diffraction. All Fe layers are found to be tetragonally strained. Moreover, a clear correlation between magnetic anisotropy and strain state is established and the magnetoelastic model proposed in Ref. 15 is clearly confirmed. Finally, the measured ratio of out-of-plane to in-plane strain clearly evidences the importance of defects and/or anharmonic effects in these films where the lattice distortion reaches values of a few percents.

EXPERIMENT

To study the dependence of the strain on the Fe film thickness, two series of samples were prepared with either $FeSi_2$ or $CoSi_2$ buffer layers. The samples, in the thickness range 0–80 ML, were grown in ultrahigh vacuum in a two-step process. First, a 1-nm-thick $FeSi_2$ (resp $CoSi_2$) template layer was grown on Si(001) by deposition of 2 ML of Fe (resp Co) at RT and subsequent annealing at 550 °C (resp 450 °C). This template largely prevents the diffusion of Si into the Fe layer and ensures epitaxial growth. Then Fe was deposited at RT with normal incidence to the desired thickness. The coverages are expressed in monolayers relative to the bcc Fe(001) surface atomic density; the nominal thickness of a ML is 0.143 32 nm without strain. Finally, the films were capped with a nonmagnetic FeSi layer (~2 nm) and with an amorphous Si layer (~2 nm) to prevent oxidation during transportation through air. A more detailed description of the sample growth and of its characterization can be found in Ref. 14.

X-ray diffraction measurements were performed on the diffraction beam line D2AM of the European Synchrotron Radiation Facility (ESRF) in Grenoble. A monochromatic x-ray beam with a 0.179 68 nm wavelength was selected by a symmetrical optics consisting of a two-crystal monochromator with sagittal focusing located between two cylindrically bent mirrors. With focusing typical angular divergences are $3.10^{-4}\times 3.10^{-3}$ rad^2 (vertical×horizontal) for a beam size of 0.3×0.3 mm^2 on the monochromator. A detailed description of the beamline can be found in Ref. 16. The samples were mounted on a seven-circle diffractometer so that the φ axis corresponds to a rotation about the Si substrate [001] direction and the χ axis is the intersection of the sample surface and the diffraction plane. The 2θ angle is as usual defined as the angle between the incident beam and the detector directions. In our experiment we used a noncoplanar arrangement where the sample normal is in a plane perpendicular to the scattering plane and makes with it an angle χ. The (004) and (202) bulk Bragg reflections of the Si substrate were used as a reference. Both perpendicular and in-plane strains of the iron films were deduced by measuring the $(202)_{Si}$ substrate and $(101)_{Fe}$ film diffraction peaks and their equivalents by 90° rotations of the sample about its normal. The maximum location of each Bragg peak was searched by iterating φ, χ, and $\theta/2\theta$ scans in the reciprocal space. We used symmetric $\theta/2\theta$ scans to ensure the local orthogonality of the scans at the peaks. The χ and φ origins were defined so that the $(004)_{Si}$ peak corresponds to $\chi=0°$, and the $(202)_{Si}$ peak to $\varphi=0$. $(101)_{Fe}$ peaks are located around $\chi=45°$ and a compressive strain in the plane comes out as an increase of χ.

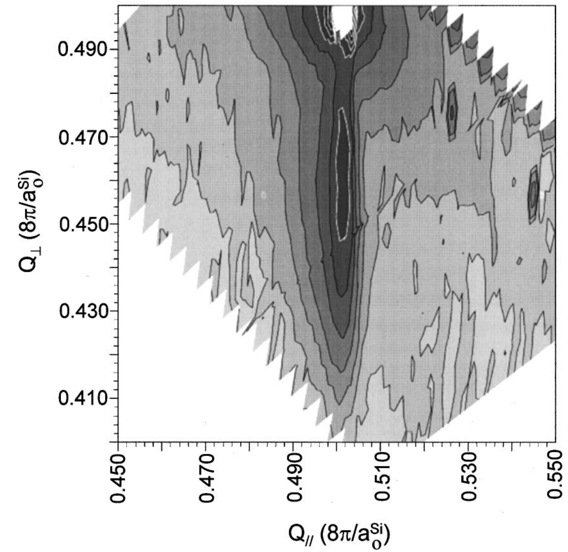

FIG. 1. A typical map of the reflected intensity distribution in reciprocal space $Q_\parallel$ and $Q_\perp$ (momentum transfert parallel and perpendicular to the surface, respectively) from a 4-ML Fe film on $CoSi_2$ template. The $(202)_{Si}$ reflection is located at $Q_\parallel=Q_\perp=0.500$, whereas the $(101)_{Fe}$ reflection from deposited Fe film is centered about $Q_\parallel=0.501$ and $Q_\perp=0.460$. $Q_\parallel$ and $Q_\perp$ are measured in units of $8\pi/a_0^{Si}$, where a_0^{Si} is the substrate lattice parameter.

RESULTS AND DISCUSSION

For some selected samples, maps of the reflected intensity distribution in reciprocal space $Q_\parallel$, $Q_\perp$ (momentum transfert parallel and perpendicular to the surface, respectively, in units of $8\pi/a_o^{Si}$) have been collected. An example is shown in Fig. 1 for a 4-ML Fe film on $CoSi_2$ template. The $(202)_{Si}$ reflection is located at $Q_\parallel=Q_\perp=0.500$, whereas the (101) reflection from deposited Fe film is centered about $Q_\parallel=0.501$ and $Q_\perp=0.460$. In this specific case the film appears to be essentially pseudomorphic. From width at half-maximum one obtains a lower limit of the coherence length along film normal of ~3.6 nm, which is much larger than the nominal Fe film thickness of 0.6 nm. Possibly the epitaxial

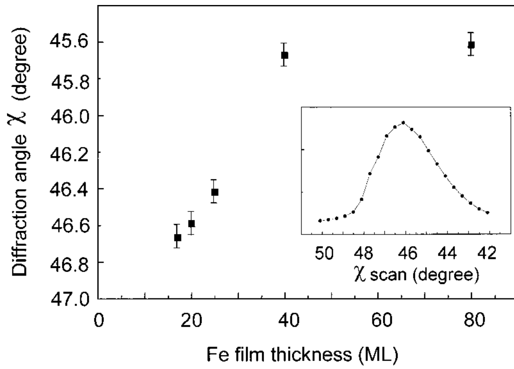

FIG. 2. Angular position of the $(101)_{Fe}$ diffraction χ peak for Fe films grown on $FeSi_2$/Si(001) substrates as a function of Fe thickness. The inset shows a typical diffraction intensity χ scan measured for a 17-ML Fe film grown at RT on $FeSi_2$/Si(001).

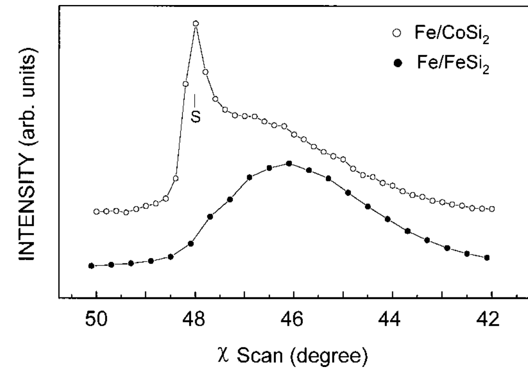

FIG. 3. Characteristic diffraction intensity χ scans measured for 17-ML Fe films grown at RT on both $FeSi_2$/Si(001) (solid circles) and $CoSi_2$/Si(001) (open circles) substrates.

FeSi protection top layer (about 3 nm thick) contributes to this coherence length. This is not unlikely, since FeSi adopts a CsCl structure that prolongs the bcc Fe structure with a very close lattice parameter. Moreover, some intermixing at Fe/FeSi interface certainly takes place and alloys with compositions ranging from pure Fe to FeSi can be stabilized in the same structure by epitaxy.[17] Hence, we restrict the following strain analysis to samples with nominal Fe thicknesses larger than 15 ML in order to minimize a possible contribution of the FeSi protection layer. Since in the present study we are mainly interested in the determination of the homogeneous (mean) strain in the thicker Fe films no attempt is made here to analyze in more detail the 4-ML data in Fig. 1 in terms of strain, coherent domain size, mosaic structure, and other kinds of defects.

Figure 2 shows the χ angular position of the $(101)_{Fe}$ diffraction peak in Fe films grown on a $FeSi_2$/Si(001) substrate as a function of the Fe thickness. For all samples, the bcc $(101)_{Fe}$ diffraction peak is quite broad with full width at half-maximum (FWHM) of about 3° (inset of Fig. 2). χ strongly depends on the thickness of the film and is larger than the 45° bulk value even in the thickest films. The peak position shifts toward lower angles with increasing Fe film thickness. Thus a clear strain is evidenced for all Fe layers. These films are obviously quite imperfect crystals as also indicated by typical rocking curves (not shown) with FWHM about 2° as compared to 0.01° for the Si substrate.

Figure 3 shows the diffracted intensity in χ scans measured on two 17-ML Fe films grown on $FeSi_2$/Si(001) and $CoSi_2$/Si(001) substrates. In the Fe layer grown on $FeSi_2$, the $(101)_{Fe}$ Bragg peak is almost symmetrical, with a ~3° FWHM, and centered at $\chi=46.2°$ whereas in the film grown on $CoSi_2$/Si(001), the peak can be clearly separated into two components: a broad peak centered at 46.8° with a FWHM of 3° and a sharp Bragg peak at 48° with a 0.6° FWHM. The same double structure has been observed in all investigated samples (6–40 ML) deposited onto $CoSi_2$ template layers. As for the Fe layers deposited on $FeSi_2$, the broader peak position shifts to lower angles with increasing layer thickness, while the sharper peak position remains almost constant. Its 0.6° FWHM suggests that this peak corresponds to a phase with a much better crystallinity. This sharp peak, which is particularly pronounced for the thinnest films, decreases in intensity and disappears for thicker films (>40 ML). Typically by 17 ML it corresponds roughly to 30% of the total reflected intensity. Its angular position corresponds closely to that expected for a pseudomorphic growth of iron on $CoSi_2$ buffer layer, as discussed below.

Accurate strain measurements have been performed by x-ray double-crystal diffractometry in a previous work on semiconductor heterostructures.[18] The method, based on relatively high index reflections is well adapted to fairly perfect semiconductor layers in the micrometer range. The present system is an ultrathin defected metal film in the nanometer range. We used the following approach that exploits the strong low-index $(101)_{Fe}$ diffraction peak.

A quantitative analysis of the φ, χ, and θ angular positions of the $(101)_{Fe}$ reflection peaks is achieved by a differential method, i.e., using the deviations $\delta\varphi$, $\delta\chi$, and $\delta\theta$ in the location of intensity maximum of the $(101)_{Fe}$ reflection relative to the $(202)_{Si}$ reflection. These quantities remain small since the lattice parameter of Fe is approximately twice that of Si.

In the operation mode of our diffractometer the general diffraction condition that the momentum transfer vector must match a reciprocal vector **H** takes the following form:

$$H_1 = H \sin\chi \cos\varphi$$

$$H_2 = H \sin\chi \sin\varphi \qquad (1)$$

$$H_3 = H \cos\chi$$

with $H=2k\sin\theta$. H_1, H_2, and H_3 and H are, respectively, the components and modulus of **H** in the sample related cubic axis of Si, $k=2\pi/\lambda$ is the modulus of incident radiation wave vector, and φ, χ, and θ are the angular positions at the maximum of the Bragg peak.

In principle, a measurement of three selected reflections gives a basis of the reciprocal lattice. This, in turn, determines the direct lattice of the homogeneously strained film and thus its deformation and/or rotation with respect to a reference structure, as described by the homogeneous tensor $\nabla\mathbf{u}$ where $\mathbf{u}$ is the displacement field. The most general form of $\nabla\mathbf{u}$ involves nine components $u_{ij}=\partial u_i/\partial x_j$, which can be

obtained most accurately from the deviations ($\delta\varphi$, $\delta\chi$, $\delta\theta$) from reference structure measured for three Bragg peaks.

For a given Bragg peak and small displacement gradient the following linear relations between the deviations $\delta\varphi$, $\delta\chi$, $\delta\theta$ and tensor components u_{ij} are obtained by differentiation of Eqs. (1) with respect to φ, χ, and θ and use of

$$\delta\mathbf{H}=\mathbf{H}'-\mathbf{H}=-\nabla(\mathbf{H}\cdot\mathbf{u}),$$

where $\mathbf{H}$ and $\mathbf{H}'$ are the reciprocal vectors of the reference and strained-rotated structure, respectively,

$$\sum_j u_{j1}\alpha_j=\alpha_2\delta\varphi-\alpha_1\alpha_3(1-\alpha_3^2)^{-1/2}\delta\chi-\alpha_1\frac{\delta\theta}{tg\,\theta}$$

$$\sum_j u_{j2}\alpha_j=-\alpha_1\delta\varphi-\alpha_2\alpha_3(1-\alpha_3^2)^{-1/2}\delta\chi-\alpha_2\frac{\delta\theta}{tg\,\theta} \quad (2)$$

$$\sum_j u_{j3}\alpha_j=(1-\alpha_3^2)^{1/2}\delta\chi-\alpha_3\frac{\delta\theta}{tg\,\theta},$$

α_1, α_2, and α_3 are the direction cosines of $\mathbf{H}$ in the cubic axis.

In the present experiment we have determined the angular deviations $\delta\varphi$, $\delta\chi$, $\delta\theta$ for (101), $(\bar{1}01)$, (011), $(0\bar{1}1)$ reflections of the Fe films. Within experimental error we find the same deviations for the four reflections, which therefore remain equivalent in the strained layer. Hence we conclude that [001] is still a fourfold symmetry axis and the most general form of the gradient tensor consistent with this symmetry is

$$\begin{pmatrix} u_{\parallel} & u_{12} & 0 \\ -u_{12} & u_{\parallel} & 0 \\ 0 & 0 & u_{\perp} \end{pmatrix},$$

i.e., a tetragonal distortion accompanied by a rotation about [001]. Now, within experimental error we further observe that

$$\delta\varphi_{(101)}=\delta\varphi_{(-101)}=\delta\varphi_{(011)}=\delta\varphi_{(0-11)}=0.$$

Hence $u_{12}=0$ and the films undergo a simple tetragonal distortion with c axis along surface normal. In the present specific case for (101), $\alpha_1=\alpha_3=1/\sqrt{2}$ and $\alpha_2=0$ we obtain from relations (2)

$$u_{\parallel}=-\delta\chi-\frac{\delta\theta}{tg\,\theta}$$

$$u_{\perp}=\delta\chi-\frac{\delta\theta}{tg\,\theta}. \quad (3)$$

This provides a measure of both in-plane ($u_{\parallel}$) and out-of-plane ($u_{\perp}$) deformation of the lattice with respect to the bulk Si lattice.

In the derivation of these relations $u_{\parallel}$ and $u_{\perp}$ are assumed to be homogeneous strain tensor components (symmetric part of displacement vector gradient) and only those terms that are first order in these strain components are retained.

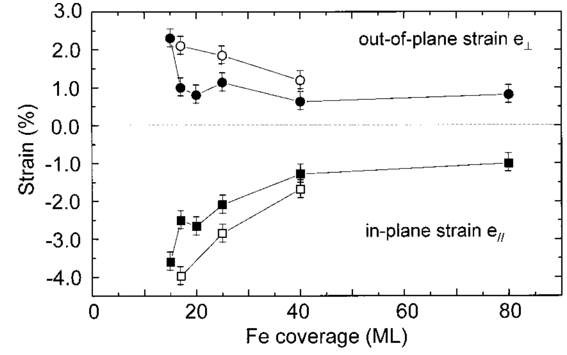

FIG. 4. Evolution of the in-plane $e_{\parallel}$ and out-of-plane $e_{\perp}$ strain components versus film thickness in epitaxial Fe films grown at RT on both $FeSi_2$/Si(001) (solid circles $e_{\perp}$ and squares $e_{\parallel}$) and $CoSi_2$/Si(001) (open circles $e_{\perp}$ and squares $e_{\parallel}$) templates. Full lines are only a guide for the eyes.

Since strains as large as $u_{\perp}=0.08$ are observed we have checked that dropping higher-order terms does not result in a significant error. Indeed, we find that the above formulas give $u_{\parallel}$ and $u_{\perp}$ with a relative accuracy, which is typically better than the experimental uncertainty in the 10% range. The latter is estimated from the width of the diffraction peaks and scatter in experimental data. Note that this does not mean that Hooke's law of linear elasticity still holds and provides a good description of the stress-strain relationship in such films by means of usual second-order elasticity constants. Indeed, as will become apparent below, our results clearly evidence a marked deviation from harmonic approximation.

The average angular positions of all four equivalent peaks are used as input in the calculation of $u_{\perp}$ and $u_{\parallel}$. The relevant strain tensor components $e_{\parallel}$ and $e_{\perp}$ with respect to unstrained Fe are deduced by $e_{\parallel}=(u_{\parallel}-u_0)/(1+u_0)$ and $e_{\perp}=(u_{\perp}-u_0)/(1+u_0)$, where u_0 is the parameter misfit.

Figure 4 shows both in-plane $e_{\parallel}$ and out-of-plane $e_{\perp}$ strain components obtained for both $FeSi_2$/Si(001) and $CoSi_2$/Si(001) templates, as a function of the Fe thickness. For $CoSi_2$, only data concerning the partially relaxed phase (broad peak in χ scan) are considered in this figure. Films grown on both substrates exhibit a similar strain behavior. The in-plane and out-of-plane strains in the Fe layer are found to be strongly thickness dependent. When the thickness of the film increases, both the in-plane and out-of-plane strains are progressively reduced. The strain ranges from values as large as -4% for $e_{\parallel}$ ($+2.6\%$ for $e_{\perp}$) in the thinnest films (<25 ML) to -1% for $e_{\parallel}$ ($\sim 1\%$ for $e_{\perp}$) in the thickest layers ($\geqslant 40$ ML). These results evidence a contraction of the Fe layer in-plane lattice parameter and an expansion of the lattice parameter in the direction perpendicular to the interface relative to the bulk in agreement with the sign of lattice mismatch $u_0=+5.6\%$. The strain relaxes rapidly towards 1% in the early stages (up to 25 ML) but note that it still remains quite large by 80 ML. The partial relaxation is usually explained in terms of misfit dislocation formation in thick films; when the residual strain is small, the activation energy to create a dislocation is too large to continue to relax the strain by this way. On the other hand, the data indicate

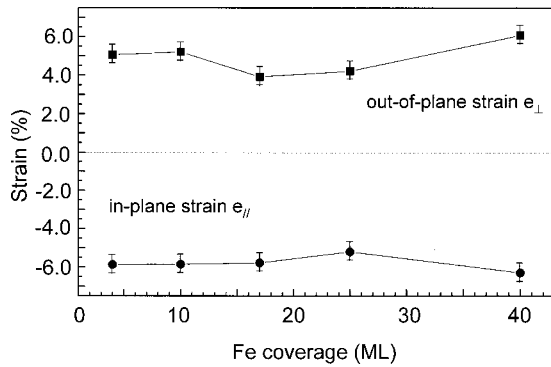

FIG. 5. Evolution of the in-plane $e_{\parallel}$ and out-of-plane $e_{\perp}$ strain components corresponding to the sharp diffraction peak (named *S* in Fig. 3) observed in the case of Fe grown at RT on $CoSi_2/Si(001)$ substrates versus film thickness.

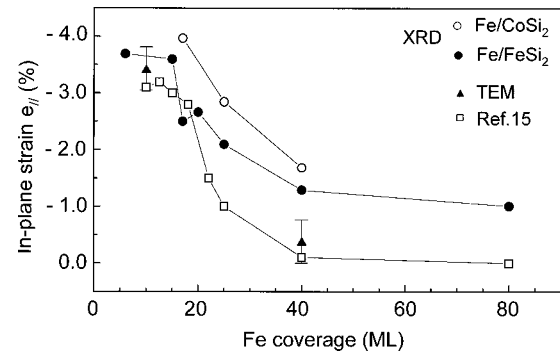

FIG. 6. In-plane strain $e_{\parallel}$ inferred from present XRD data compared with those deduced from previous magnetic and TEM measurements (Ref. 15).

that strict pseudomorphic growth does not occur even in the thinnest films investigated, since one still observes that $|e_{\parallel}| < u_0$. It is also clear from Fig. 4 that substantial differences appear between the two templates. Indeed, for a given thickness, the strain in Fe film grown on the $CoSi_2$ buffer layer is systematically larger than in the film grown on $FeSi_2/Si(001)$ substrate. Obviously the strain relaxation is clearly correlated to the nature of the buffer layer and, in particular, its morphololgy.

Concerning the additional sharp peak observed in the case of Fe grown on $CoSi_2/Si(001)$ substrates and essentially visible in the thinnest films, the corresponding in-plane and perpendicular strain components do not change versus Fe film thickness (Fig. 5). Since the strain component $e_{\parallel} \cong -u_0$ the lattice misfit, we tentatively attribute it to diffraction from (101) planes of an essentially perfect pseudomorphic bcc Fe phase that forms in the thinnest layers only. For 4 ML Fe, where only the sharp Bragg peak is observed, we assume that the whole Fe layer is completely coherent with the $CoSi_2$. Thus, in the earlier growth stages the films exhibit an exceptionally large strain. For increasing Fe layer thickness, a fraction of the film seems to relax to a more bulklike bcc lattice. As a result, the {101} Bragg diffraction peaks now display two components, a sharp one associated with pseudomorphic Fe growth and a larger one corresponding to partially relaxed Fe. For Fe layers grown on $FeSi_2$, we could never observe such a pseudomorphic component irrespective of the film thickness. So, the $CoSi_2$ template permits to grow a nearly perfect coherent phase of Fe in contrast to the $FeSi_2$ buffer. Moreover, the partial relaxation of the dominant phase in thicker films (the broader peak in χ scans) is always substantially more pronounced on $FeSi_2$ than on $CoSi_2$ templates. A detailed knowledge of surface structural properties of the template layer is obviously essential to precisely predict and control the strain state of the Fe films. Possibly, a scanning tunneling microscopy (STM) study might shed more light on the morphology of both template layers that govern the growth of the iron layer.

We now discuss the point that initiated the present strain measurements, namely, the relationship between Fe film strain and observed magnetic anisotropy versus film thickness. In a previous work,[15] we showed that Fe films deposited at normal incidence exhibit simple in-plane fourfold anisotropy. The relevant fourth-order effective anisotropy constant K_4^{eff} varies strongly with film thickness and changes its sign around a critical thickness of around 20 ML, which causes a switch of the easy axis from [100] to [110] direction of the bcc Fe structure. This behavior was attributed to the combined result of the tetragonal strain, silicon content, and interface effect.[15] More precisely, it was shown that the dominant effect responsible for this remarkable behavior must be related to fourth-order (in-spin) magnetoelastic effects due to a large biaxial in-plane compressive strain in the film. A pair-interaction model of the type proposed by Néel[19] and linear elastic theory were used to estimate the in-plane $e_{\parallel}$ strain component needed to produce the measured values of K_4^{eff} as a function of the layer thickness.[15]

In Fig. 6 we compare the in-plane strain $e_{\parallel}$ inferred in this way from magnetic measurements, with present data obtained by XRD measurements. As can be seen, one observes a reasonable agreement in both the sign and the magnitude of the $e_{\parallel}$ strain though it is apparent that the $e_{\parallel}$ estimated from magnetic anisotropy are systematically smaller than those obtained by XRD. On the one hand, the difference can be traced back to uncertainties in the Néel model due to the fact that precise values of some parameters, such as magnetoelastic coupling constants, were not available and could only be estimated approximately. On the other hand linear elasticity theory was used in Ref. 15 and the ratio of out-of-plane to in-plane strain components calculated by mean of $e_{\perp}/e_{\parallel} = -2C_{12}/C_{11} = -1.17$, i.e., with usual second-order elasticity constants C_{12} and C_{11} from Fe bulk as measured by elastic wave propagation techniques. Now the strains involved in these techniques are in the $10^{-4}-10^{-3}$ range rather than in the few percent range observed in epitaxial Fe. Hence, higher-order anharmonic effects might be important in such films. Moreover, deviations from bulk elastic properties might be expected due to the presence of various kinds of defects in the film, such as, small coherent domains, inhomogeneous strains, dislocations, and defected regions of the film. Such deviations can be seen clearly in Table I which summarizes the experimental XRD value of the $e_{\perp}/e_{\parallel}$ ratio. As can be seen, this ratio is not constant but depends on the Fe film thickness and differs markedly from the value expected from linear elastic theory, in particular, in the thinnest

TABLE I. Experimental XRD value of the $e_\perp/e_\parallel$ ratio.

	Fe coverage (ML)	15	17	20	25	40	80
$\frac{e_\perp}{e_\parallel}$	Fe/$FeSi_2$	−0.64	−0.40	−0.30	−0.54	−0.48	−0.80
	Fe/$CoSi_2$		−0.53		−0.65	−0.70	

film where the strain is largest. It is apparent that the abovementioned effects decrease the Poisson-like distortion, i.e., $|e_\perp/e_\parallel|$ is smaller than in the linear regime. When this decrease in $|e_\perp/e_\parallel|$ ratio is taken into account in the Néel model the $e_\parallel$ values estimated from magnetic anisotropy increase substantially and are now essentially identical to those inferred from XRD in Fig. 3.

Thus, the present XRD data clearly confirm that the origin of the remarkable magnetic anisotropy behavior observed for Fe layers deposited at normal incidence results basically from magnetoelastic coupling associated with a strong tetragonal distortion of the cubic iron structure as discussed in Ref. 15.

Finally, in the latter work, the critical thickness for easy magnetic axis switch over to bulklike directions was found to depend markedly on the nature of the template layer. For Fe films grown on $CoSi_2$ this transition is shifted to larger thicknesses with respect to the films grown on $FeSi_2$ template: We found 18 ML on $FeSi_2$, as compared to 22 ML on $CoSi_2$. It is now clear that this difference is a direct consequence of the different strain state on $FeSi_2$ and $CoSi_2$ templates as evidenced in the present work and shown in Fig. 4. For a given thickness, Fe films grown on the $CoSi_2$ are found to be systematically more strained than those deposited on $FeSi_2$. So, the recovery of a bulklike anisotropy takes place at a larger thickness on the $CoSi_2$ template. Again this result provides nice support to the magnetoelastic model in Ref. 15.

CONCLUSION

The strain in a series of Fe films on Si(001) has been studied using x-ray diffraction. Perpendicular and in-plane strains of the Fe films have been measured in order to test the magnetic anisotropy model proposed in Ref. 15. We find that the origin of the in-plane magnetic anisotropy behavior in such films can be unambiguously accounted by fourth-order magnetoelastic effects arising from a strongly thickness-dependent tetragonal strain.

*Corresponding author: FAX: 03 89 33 60 83. Email address: P.Wetzel@uha.fr

[1] G. A. Prinz, in *Ultrathin Magnetic Structures*, edited by H. Heinrich and J. A. C. Bland (Springer-Verlag, Berlin, 1994), Vol. 2, pp. 1–44.
[2] G. A. Prinz, Science **282**, 1660 (1998).
[3] A. Hirohata, Y. B. Xu, C. M. Guertler, J. A. C. Bland, and S. N. Holms, Phys. Rev. B **63**, 104425 (2001), and references therein.
[4] G. A. Prinz, J. Magn. Magn. Mater. **200**, 57 (1999).
[5] R. Fiederling, M. Keim, G. Reuscher, W. Ossau, A. Waag, and L. W. Molenkamp, Nature (London) **402**, 787 (1999).
[6] Y. Ohno, D. K. Young, B. Beschoten, F. Matsukura, H. Ohno, and D. D. Awschalom, Nature (London) **402**, 790 (1999).
[7] R. Kläsges, C. Carbone, W. Eberhardt, C. Pampuch, O. Rader, J. Kachel, and W. Gutat, Phys. Rev. B **56**, 10 801 (1997).
[8] J. Alvarez, J. J. Hinarejos, E. G. Michel, G. R. Castro, and R. Miranda, Phys. Rev. B **45**, 14 042 (1992).
[9] K. Rührnshopf, D. Borgmann, and G. Wedler, Thin Solid Films **280**, 171 (1996).
[10] J. M. Gallego, J. M. Garcia, J. Alvarez, and R. Miranda, Phys. Rev. B **46**, 13 339 (1992).
[11] E. Kneller, *Ferromagnetismus* (Springer-Verlag, Berlin, 1962), pp. 148, 196, 197, 224, 260.
[12] D. Berling, G. Gewinner, M. C. Hanf, K. Hricovini, S. Hong, B. Loegel, A. Mehdaoui, C. Pirri, M. H. Tuilier, and P. Wetzel, J. Magn. Magn. Mater. **191**, 331 (1999).
[13] P. Bertoncini, P. Wetzel, D. Berling, G. Gewinner, C. Ulhaq-Bouillet, and V. Pierron-Bohnes, Phys. Rev. B **60**, 11 123 (1999).
[14] P. Bertoncini, D. Berling, P. Wetzel, A. Mehdaoui, B. Loegel, G. Gewinner, C. Ulhaq-Bouillet, and V. Pierron-Bohnes, Surf. Sci. **454-456**, 755 (2000).
[15] P. Bertoncini, P. Wetzel, D. Berling, A. Mehdaoui, B. Loegel, G. Gewinner, R. Poinsot, and V. Pierron-Bohnes, J. Magn. Magn. Mater. **237**, 191 (2001).
[16] J. L. Ferrer, J. Synchrotron Radiat. **5**, 1346 (1998).
[17] S. Hong, P. Wetzel, G. Gewinner, D. Bolmont, and C. Pirri, J. Appl. Phys. **78**, 5404 (1995).
[18] L. De Caro, C. Giannini, and L. Tapfer, J. Appl. Phys. **79**, 4101 (1996).
[19] L. Néel, J. Phys. Radium **15**, 225 (1954).